JGR Space Physics

RESEARCH ARTICLE
10.1029/2020JA028359

A Statistical Study of Polar Cap Flow Channels and Their IMF By Dependence

K. Herlingshaw[1,2], L. J. Baddeley[1,2], K. Oksavik[1,2], and D. A. Lorentzen[1,2]

[1]Department of Arctic Geophysics, University Centre in Svalbard, Longyearbyen, Norway, [2]Birkeland Centre for Space Science, University of Bergen, Bergen, Norway

Key Points:
- We present the statistics of flow channels in the dayside polar cap area including duration, width, peak velocity, and monthly occurrence
- Their formation is intimately related to IMF By, and the flow channels shift dawnward/duskward for +By/−By
- Higher velocity flows in the polar cap concentrate into localized, narrower channels

Supporting Information:
- Supporting Information S1

Correspondence to:
K. Herlingshaw,
katie.herlingshaw@unis.no

Citation:
Herlingshaw, K., Baddeley, L. J., Oksavik, K., & Lorentzen, D. A. (2020). A statistical study of polar cap flow channels and their IMF By dependence. *Journal of Geophysical Research: Space Physics*, *125*, e2020JA028359. https://doi.org/10.1029/2020JA028359

Received 17 JUN 2020
Accepted 25 SEP 2020
Accepted article online 17 OCT 2020

Abstract An algorithm to detect high-speed ionospheric flow channels (FCs) in the polar cap was applied to data from the Longyearbyen radar of the Super Dual Auroral Radar Network. The Longyearbyen radar is at high latitude (78.2°N, 16.0°E geographic coordinates) and points northeast; therefore, it is in an ideal position for measuring zonal flows in the polar cap. The algorithm detected 998 events in the dayside polar cap region over 2 years of observations. The detected FCs typically were between 200 and 300 km latitudinal width, 1.1–1.3 km s^{-1} peak velocity, and 3 min in duration. The FC location shows an interplanetary magnetic field (IMF) By dependency, moving dawnward/duskward for a +By/−By. The FC monthly occurrence shows a bimodal distribution with peaks around the spring and autumn equinoxes, likely due to increased coupling between the solar wind-magnetosphere-ionosphere system at these times. The highest peak velocities show an absence of broad FC widths, suggesting that as the flow speed increases in the polar cap, the channels become more localized and narrow.

1. Introduction

The shape and flow strength of the large scale high-latitude plasma convection is strongly governed by the interplanetary magnetic field (IMF) (Cowley & Lockwood, 1992). Under southward IMF, magnetic reconnection occurs at the dayside subsolar point due to the merging of antiparallel magnetic fields. This reconnection drives antisunward flows across the polar cap, and reconnection in the Earth's magnetotail drives sunward return flows at lower, subauroral latitudes (Dungey, 1961). Dayside reconnection is the dominant mechanism by which energy and momentum are transferred from the solar wind to the Earth's magnetosphere and ionosphere (Pinnock et al., 1993). In the ionosphere, the resultant motion due to dayside and nightside reconnection under IMF Bz− conditions is visualized as a twin cell ionospheric convection pattern. Statistical convection models have been developed to predict the convention pattern using a variety of techniques and observations, including satellite measurements (Heelis, 1984; Heppner & Maynard, 1987) and incoherent scatter radars (Cousins & Shepherd, 2010; Pettigrew et al., 2010; Ruohoniemi & Greenwald, 2005; 1996; Thomas & Shepherd, 2018). For IMF By dominant conditions, the reconnection location at the magnetopause boundary is shifted to earlier or later magnetic local time (MLT) locations. The twin cell pattern becomes twisted, forming a dominant round cell extending over the majority of the polar cap adjacent to a thin, crescent-shaped cell. The orientation of the IMF By− component determines the location of each of the cells. For IMF By+ the larger, dominant cell lies on the dusk side of the polar cap and the crescent cell on the dawnside of the polar cap. The dayside convection throat and cusp are shifted postnoon, and the tension imposed on the field lines leads ionospheric flows with an westward component. For IMF By−, the orientation of the cells is reversed, the dayside convection throat and cusp are shifted prenoon, and the ionospheric flows have an eastward component.

Plasma is transported across the polar cap along the streamlines of the convection pattern at typical speeds of several hundred meters per second (MacDougall & Jayachandran, 2001; Oksavik et al., 2010). Within the dayside cusp region, flows of enhanced velocities (~>1 km s^{-1}) have been observed and named differently depending on the parameter in which they were identified. These phenomena include flow channels/bursts, pulsed ionospheric flows (PIFs), poleward moving auroral forms (PMAFs), and poleward moving auroral radar forms (PMRAFs) (see Davies et al., 2002). These signatures are all related and are the ionospheric manifestation of reconnection at the dayside magnetopause and flux transfer events (Haerendel et al., 1978; Russell & Elphic, 1978, 1979; Oksavik et al., 2004). When dayside reconnection occurs, flow channels are

thought to be an important feature for the injection of corotating plasma from the subauroral plasma reservoir into transpolar flow (Carlson et al., 2006) and in the structuring of plasma within polar cap patches in their early formation stages (Carlson, 2012). Dayside flow channels have also been found to be collocated with airglow patches, forming under By-dominated dayside reconnection and potentially transporting the airglow patches across the polar cap and into the nightside auroral zone (Hosokawa et al., 2019; Nishimura et al., 2014). Flow channels have been observed deep within the polar cap on the dawn/dusk flanks and on the nightside due to magnetotail reconnection and substorms (Nishimura et al., 2010; Oksavik et al., 2010; Sandholt & Farrugia, 2009).

In this study, we are concerned with the flow channels in the dayside cusp region, coupling strongly with the solar wind. Flow channels of this kind were first observed by the PACE HF radar by Pinnock et al. (1993) and named flow channel events. Flow channel events were consistent with the magnetic tension force on newly opened field lines and created longitudinally extended fast flows. Provan et al. (1999) further researched these events and found them to be quasiperiodic, terming them PIFs. They observed PIFs within data from the Super Dual Auroral Network (SuperDARN) and found that they occurred between 0250 and 1650 MLT with a peak between 0900 and 1210 MLT, 76 and 82 MLAT, and a typical recurrence rate of 7–8 min. They also observed an IMF By dependence on the location and frequency of the PIFs, with the location of the PIFs shifting postnoon/prenoon for positive/negative IMF By. Rinne et al. (2010, 2011) observed a series of flow channels moving with the ionospheric convection into the polar cap. The zonal flow direction in these events aligned with the tension applied by the IMF By component, which sharply changed direction multiple times during the observations. Each flow channel propagated poleward, remaining separated from the neighboring channels with flow directions consistent with the tension applied by IMF By polarity changes. These observations support the view that a flow channel is formed near the polar cap boundary during dayside reconnection and that these flow channels will remain separate and push each other into the polar cap while the magnetic tension force and its associated field-aligned current system are maintained (Lockwood et al., 2001; Moen et al., 2013).

Flow channels can be divided into four categories based on the location of the magnetic field line within the Dungey (1961) convection cycle (Andalsvik et al., 2011; Sandholt & Farrugia, 2009; Sandholt, Andalsvik, et al., 2010). The categories of the flow channels excited by the magnetic field lines at different stages are as follows: newly open field lines (FC 1), old open field lines (FC 2), and field lines connected to the tail lobes (FC 3), and field lines connected to the plasma sheet (FC 4). The focus for this paper is on dayside flow channels so will concern FC 1 and FC 2. FC 1 and FC 2 both occur on open field lines and flow antisunward but are distinguished by the amount of time that has passed since the driving dayside reconnection happened. FC 1 occur on newly open field lines (less than 10 min since reconnection), are associated with PIFs and the early stages of PMAFs/PMARFs, and are characterized by noonward convections in the prenoon and postnoon sectors. FC 2 occur on old open field lines (10–20 min since magnetopause reconnection) embedded in polar rain precipitation, are located near the duskside or dawnside of the polar cap boundary, and are associated with the highest-latitude stages of PMAFs/PMARFs (Sandholt, Farrugia, et al., 2010).

While the study by Provan et al. (1999) identified flow channel-like features (i.e., PIFs) in the Finland SuperDARN radar, they did not stipulate that the feature had to be embedded within a discernible background flow. In this study, we identify flow channels which are embedded in a discernible background flow and explore their relationship to IMF By. We apply the flow channel detection algorithm from Herlingshaw et al. (2019) to 2 years of SuperDARN data from the Longyearbyen radar. The statistical characteristics of the detected flow channels are examined including the duration, width, peak velocity, and monthly occurrence. The solar wind driving conditions are investigated, as is the dependence of the flow channels on IMF By and the critical clock and regime for flow channel formation.

2. Instrumentation

The SuperDARN is a chain of high-frequency radars whose field of view (FOV) collectively cover large regions of the polar ionospheres in both hemispheres (Chisham et al., 2007; Greenwald et al., 1995). Each SuperDARN radar is frequency agile (8–20 MHz) and measures the line-of-sight Doppler velocity, spectral width, and backscatter p ower from decameter-scale ionospheric irregularities at E and F region altitudes. These irregularities can be used as markers to accurately measure the ionospheric convection velocity.

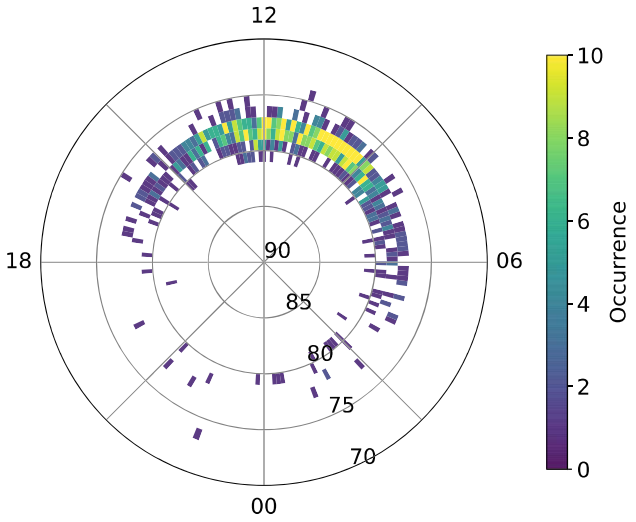

Figure 1. Occurrence distributions in MLAT/MLT coordinates binned into 1° by 2° bins of the flow channel center at the beginning of each event within the study.

In this study, we use 2 years of data (October 2016 to November 2018) from the Longyearbyen (LYR) SuperDARN radar, located at 78.153°N, 16.074°E, 472 m altitude. This radar was selected as its FOV covers a large area of the polar cap, including the dayside cusp region, regularly recording data up to 1,500 km in range (with a largest possible range of 3,500 km) and a latitudinal span of approximately 76–82° (magnetic coordinates). This latitudinal range is statistically located in the polar cap, as it is poleward of the average location of the open-closed field line boundary at 75° (Yeoman et al., 2002). In common mode of operation, the radar beam is steered through 16 positions with an azimuthal separation of 3.24° with a 1 min resolution. Each radar beam contains 75 range gates with a distance to the first range gate of 180 km and a range resolution of 45 km.

Solar wind velocity and IMF By and Bz components (GSM) were obtained from NASA's Goddard Space Flight Center OMNI data set through OMNIWeb. The data have been time shifted to Earth's bow shock.

3. Method

In this statistical study, we use the algorithm described by Herlingshaw et al. (2019) to automatically detect flow channels in SuperDARN LYR data over a 2 year period from October 2016 to November 2018. Examples of flow channels detected with the algorithm can be seen in Herlingshaw et al. (2019) (Figures 1 and 3) and in the supporting information of the current paper. Here, we summarize some of the key features of the algorithm. The algorithm identifies velocity structures with average magnitudes over 900 m s^{-1}. These velocity structures must be embedded within a slower moving background flow with sharp gradients on the edges of the flow channel. The algorithm searches for sharp gradients of opposing signs on the edges of the flow channel with magnitudes of at least 400 m s^{-1} $cell^{-1}$. The background flows do not include any velocities exceeding 900 m s^{-1} as it should be moving slowly with respect to the flow channel. Principle component analysis and ellipse fitting were used to determine the width and orientation of the flow channel. The algorithm uses a 3 min average of 1 min resolution common mode data in order to increase the coverage of the received backscatter. The detections are then split into events, which are classified as a continuous detection of a flow channel with no time gaps greater than 3 min. For a more detailed explanation of the algorithm, see Herlingshaw et al. (2019).

A total of 1,048 events was identified during this period. We will investigate the characteristics of the flow channels including location, duration, width, peak velocity, and IMF By dependence. All of these properties are outputs of the algorithm, except for the IMF By dependency. We define the IMF clock angle (θ) as

$$\theta = \tan^{-1}\left(\frac{B_y}{B_z}\right), \quad (1)$$

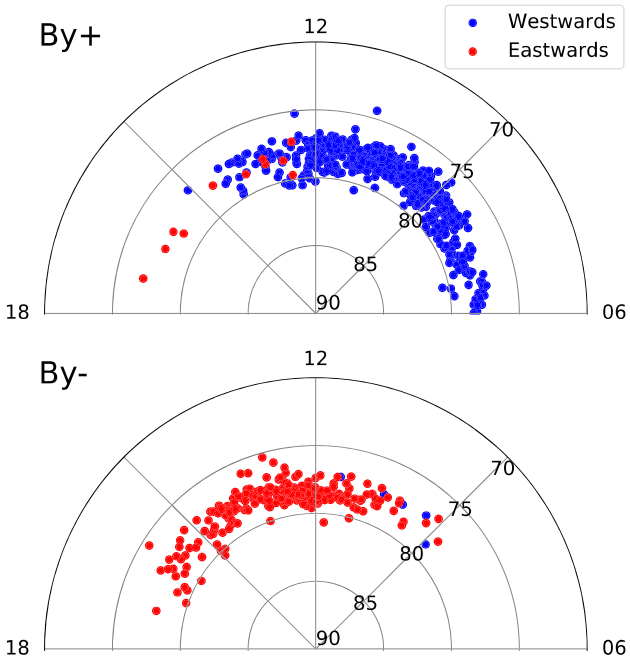

Figure 2. Occurrence distributions in MLAT/MLT coordinates for (top) IMF By+-dominated and (bottom) IMF By−-dominated solar wind conditions. Filled circles represent the direction of the plasma flow within the channel center at the beginning of each event, where blue and red indicate flows westward (toward) and eastward (away) from the Longyearbyen radar, respectively.

where θ ranges from 0–360°. The clock angles were used to separate the IMF into By− dominant ($225° < \theta < 315°$) and By+ dominant ($45° < \theta < 135°$). Reconnection bursts at the magnetopause take place for a wide range of clock angles (30° to 330°) (Neudegg et al., 2000). We expect to observe reconnection-driven dayside signatures within our By+ and By−dominated regimes as they are within this range.

4. Results and Analysis

The first statistical characteristic of the flow channels examined was the flow channel MLAT/MLT location. Figure 1 shows occurrence distribution of the flow channel centers at the beginning of each event on a polar grid. The distribution is plotted in MLAT/MLT coordinates in 1° by 2° bins. The majority of flow channels were detected on the dayside, with the densest population in the prenoon sector between 9 and 12 MLT. There are also events present on the flanks and nightside in smaller abundances. These results indicate that the location of the Longyearbyen radar is favorable for detecting plasma accelerated to high speeds within the dayside cusp region, likely due to dayside reconnection. The small occurrence of nightside flow channels could be due to the FOV of the radar being too far north in order to identify nightside reconnection-driven channels.

In this paper we are concerned with FCs occurring on the dayside; therefore, the detected events were filtered by MLT ($6 \leq MLT \leq 18$). From this point on, the analysis will focus on the 998 dayside events. Solar wind orientation is a key driver of the dayside reconnection which drives the high-latitude convection and thus is intimately linked to dayside flow channels. To explore these driving conditions, the IMF was averaged 10 min before each event and the clock angle calculated using Equation 1. There was no restraint on the stability of the IMF, so our sample includes both periods of stable and variable IMF.

Figure 2 shows the MLT/MLAT distribution of the flow channel centers at the beginning of each event for IMF By+ (top)- and By− (bottom)-dominated regimes. Blue filled circles mark plasma flows within the channels moving toward the radar and red mark plasma flows within the channels moving away from the radar. As the Longyearbyen radar FOV is orientated toward the North East, the red points indicate an eastward component of flow while the blue indicates a more westward component. The flow channels show a

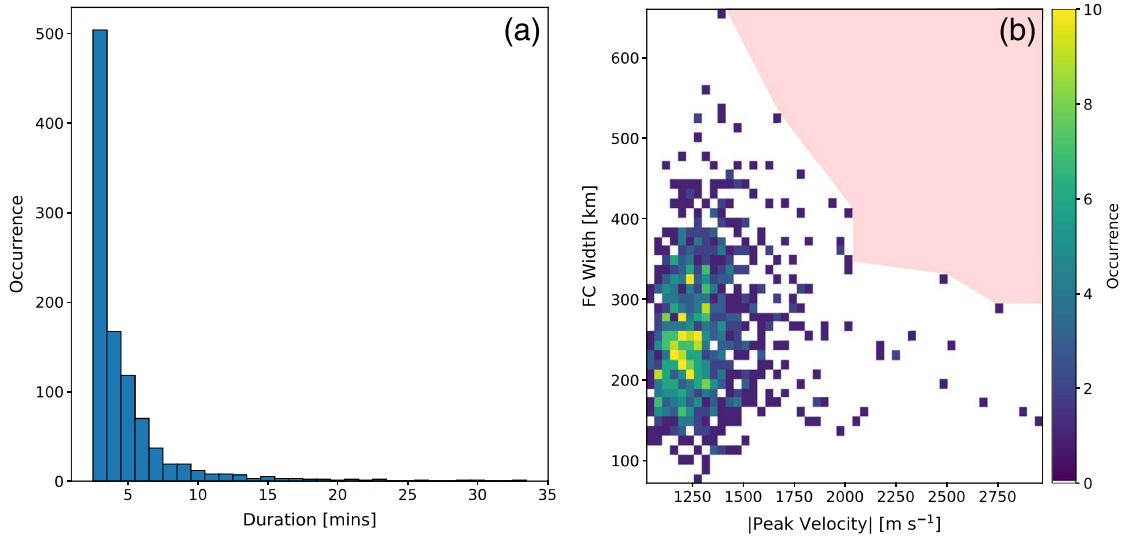

Figure 3. Distributions of (a) flow channel duration and (b) flow channel width against the magnitude of the peak flow channel velocity.

distinct dependence on IMF By where the flow channel location is shifted dawnward for By+ and duskward for By−. This is the opposite direction to where the mapped footprint of the reconnection region is displaced in each case.

In addition to the location of the flow channels, the duration, FC width, and peak velocity of the detected flow channels were also investigated, as shown in the distributions in Figures 3a and 3b. As each scan is a 3 min average, Figure 3a shows that 49% of the 998 events were detected for the minimum possible duration. There are however a small subset (6%) of stable events that last over 10 min. Figure 3b shows that the flow channels range between 72 to 660 km width and peak velocities of 1–3 km^{-1}. The densest population of flow channels ranges between 200 and 300 km width peak velocities of 1.1–1.3 km s^{-1}. There is also a fast population that travels over 1.5 km s^{-1} (12%).

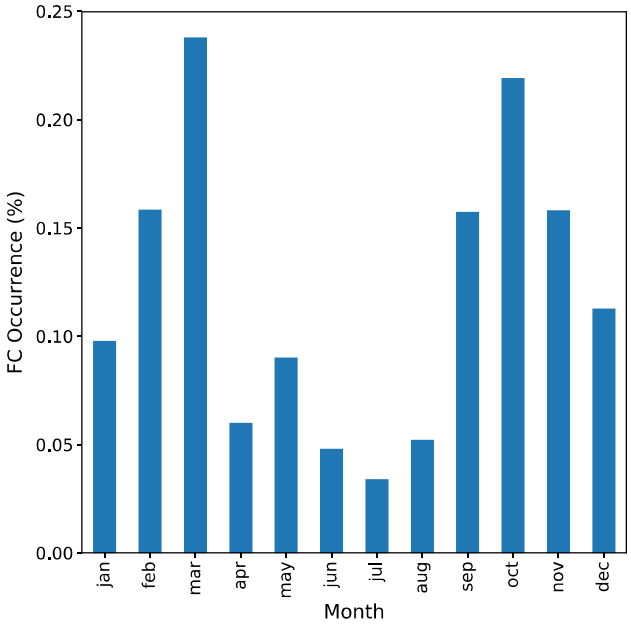

Figure 4. Monthly dayside flow channel occurrence normalized to monthly operational radar time on the dayside (06 ≤ MLT ≤ 18).

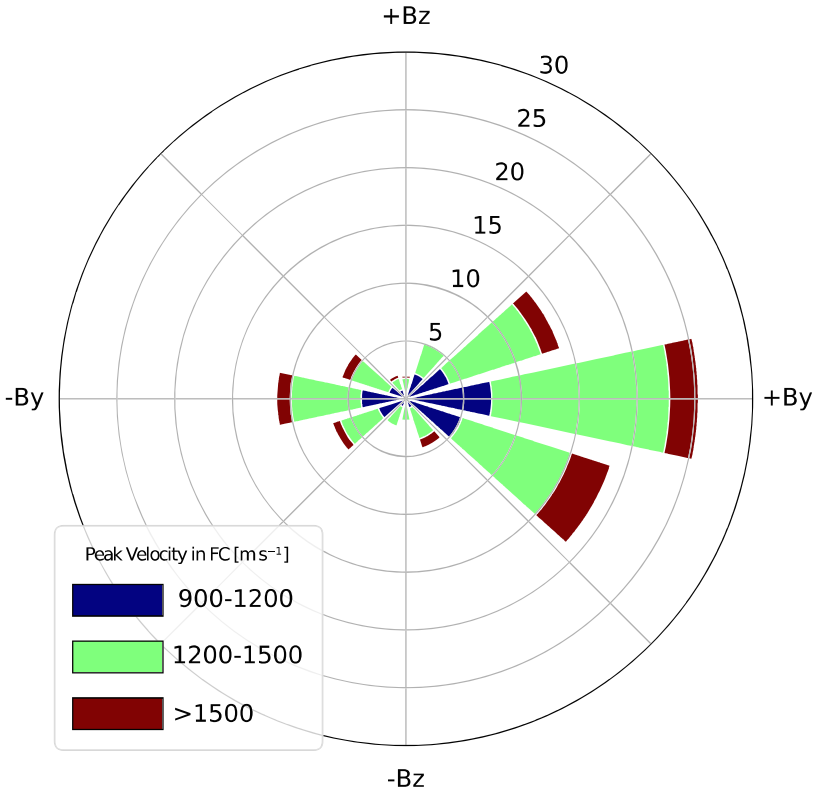

Figure 5. Wind rose diagram showing 30° wide solar wind clock angle radial spokes, colored to peak flow channel velocity magnitudes of 900–1,200 m s^{-1} (blue), 1,200–1,500 m s^{-1} (green), and >1,500 m s^{-1} (red). The radial axis shows the percentage of flow channel occurrence, increasing in 5% increments.

Figure 4 shows the monthly flow channel occurrence normalized to the monthly operational radar time for the 2 year interval. The distribution shows a clear bimodal signature, where the distribution peaks in March and October, close to the spring and autumn equinoxes.

Figure 5 shows the distribution of IMF clock angles at the beginning of each flow channel event. Each radial spoke shows the percentage of flow channel events within a 30° range of clock angles. The colored bins within each spoke show the magnitude of the peak velocity within the flow channels at the beginning of each event. The flow channels show a clear IMF By dependency, as the occurrences rise toward By dominant angles and fall toward Bz dominant angles. There are 554 By+ events, 227 By−, 86 Bz+, and 89 Bz− events. There were no corresponding IMF data for 42 of the FCs, so it was not possible to include these events in the analysis of the IMF By dependence. The higher number of By+ events could be a result of reconnection in the By+ configuration drawing in plasma from the postnoon sector, which has been illuminated longer by the solar radiation. The plasma in the postnoon sector has consequently been ionized more and is denser, so it creates more ionospheric irregularities for the SuperDARN radar to measure and we can therefore easily measure the flow channels in these driving conditions (Koustov et al., 2019).

Other relations were investigated but not displayed in this paper as there were no clear relationships. For example, there was no obvious link between the magnitude of flow velocity on the MLT location or the magnitude of IMF By and the flow velocity.

5. Discussion

The first statistical study on polar cap flow channels within Longyearbyen SuperDARN data was conducted to provide quantitative insight regarding the mesoscale flow structures embedded within the large-scale ionospheric convection. Our algorithm has the capability to detect flow channels at all MLT/MLATs measured by the LYR radar. The algorithm identifies flow channels with average speeds over 900 m s^{-1}, embedded in background flows moving at least 400 m s^{-1} slower with sharp gradients on either side of the

channel. Most flow channels were detected on the dayside, peaking between 9 and 12 MLT, with scattered events on the flanks and nightside. To investigate the dayside-driven channels, the events were filtered to include only those between 6–18 MLT.

5.1. Duration of Zonal Flow Channels

Dayside flow channels have previously been estimated to range from 5–25 min in duration (Lockwood et al., 1990). Almost half (49%) of flow channels were detected for the minimum possible duration of 3 min. To create sufficient scatter to detect a FC, the radar requires ionospheric irregularities and the correct ionospheric propagation conditions. The algorithm has a high threshold value of 900 m s^{-1} and many other restraints that require high flow values within the FC, low background flow values, and sharp gradients between the two. Therefore, the most common duration of 3 min is likely an underestimation of the actual duration of the channels, due to instrumentation effects and the stringent conditions of the algorithm. We likely detect the FC at its peak but may not record it during the entire formation and decay process, when the channel is turbulent and not well defined (as seen in the case studies in Herlingshaw et al., 2019).

Figure 1 shows that the algorithm detects FCs both in the dayside cusp and throat region (FC 1 on newly opened field lines), all the way around to the dawn and dusk flanks (FC 2 on old-opened field lines). We see temporal variability in both of these types of FC, as they rise above the threshold level and then fall back below it, like a transient pulse. Provan et al. (1999) observed pulsed transients poleward of the convection reversal boundary with a recurrence rate of 7–8 min. The FCs deeper into the polar cap, on old open field lines, have mainly been studied with single defense meteorological satellite program (DMSP) satellite passes (Sandholt & Farrugia, 2009), so it was not possible to detect variation in the FCs. Our method reveals that there is a high degree of temporal variation in the FC on old open flux in the polar cap, which is consistent with a case study of Oksavik et al. (2010).

5.2. Width and Peak Velocity of Zonal Flow Channels

The Longyearbyen radar look direction is most favorable to detect longitudinally orientated flow channels. We therefore primarily measure the latitudinal width of the channel, which spans over a few beams, and cannot detect the longitudinal width of the channel if it extends out of the radar FOV. Figure 3 shows that the flow channels were mostly between 200 and 300 km in latitudinal width with peak velocities of 1.1–1.3 km s^{-1}. The width values are of a similar order to previous studies, such as Pinnock et al. (1993) (100 km), Provan et al. (1998) (250 km), Wang et al. (2016) (300 km), and Zou et al. (2015) (200–300 km).

The interesting result regarding these FC characteristics involves the red-shaded area in Figure 3. This area is void of data, pointing to an absence of fast, wide FCs. This is not true for the most densely populated area of the distribution (1.1–1.3 km s^{-1}), where there is a large spread in widths. This suggests that high-velocity flows in the polar cap seem to concentrate and be localized into narrower channels. However, the population of flow channels with very high speeds (>1,500 m s^{-1}) and large widths (>500 km) is small, so the exact relationship requires further study to be confirmed.

5.3. IMF By dependence of Zonal Flow Channels

Figures 2 and 5 clearly show that the flow channel location and direction have an IMF By dependence. The flow channel location is pushed dawnward for IMF By+, and mostly westward flows are observed on the dayside, while for IMF By− the flow channel location is pushed duskward and mostly eastward flows are observed. This IMF By dependence is consistent with statistics of other phenomena linked to flow channels such as PIFs (Provan et al., 1999), PMAFs (Karlson et al., 1996), airglow patches (Wang et al., 2016), and polar cap patches (Spicher et al., 2017). Provan et al. (1999) suggest that for IMF By+, the cusp and dayside merging gap are shifted postnoon and cusp precipitation occurring immediately downstream will be shifted prenoon. Under the influence of the tension applied to the field lines, the FC will flow predominantly westward into the dawn sector. The opposite will occur for IMF By−, and this is consistent with the trends in Figure 2. The main statistical study relating to SuperDARN observations of PIFs by Provan et al. (1999) used the SuperDARN radar located in Finland with a FOV pointing toward North. The Longyearbyen field of view (pointing mostly Eastward) is orientated much more favorably to detect the zonal flows associated with the tensions of a nonzero IMF By component. The position of the LYR radar at 78° latitude is also more ideal than the Finland radar (located at 62° latitude) for detecting FCs on newly opened field lines, as the LYR radar rotates underneath the cusp and dayside reconnection region. Our algorithm also uses the entire field of view to automatically detect 998 events over a 3 year period, while Provan et al. (1999) used a two-beam swinging

technique to manually identify 31 days with PIF activity. Using the entire FOV allows us to confidently detect FCs embedded within a slower moving background flow.

The dependency on IMF Bz shows that in the absence of a significant IMF By component, the distribution is more centered around noon in the IMF Bz−-dominated case (not shown) as the reconnection region has not been shifted dawnward or duskward. However, the SuperDARN Longyearbyen radar has a look direction primarily east-west. This orientation is not favorable to measure any high-velocity antisunward (northward) components of flow present during IMF Bz− dominant conditions, which would flow perpendicular to the radar beams. Only 9% of the flow channels were detected under predominant IMF Bz+ conditions, and the distribution in MLAT/MLT (not included) shows no clear relationship, possibly due to complicated flow ionospheric patterns resulting from lobe reconnection.

The majority of detected flow channels (78%) were under By dominant conditions. As stated, the look direction of the SuperDARN Longyearbyen radar could be biasing these results, as it is orientated in a favorable direction to detect zonal flow channels. However, Wang et al. (2016) also find that they detect flow channels associated with airglow patches most frequently during IMF By dominant conditions. In that study, satellite data were used to determine the flow characteristics, removing the look direction bias that applies to single SuperDARN radars and still noting the same IMF By dependence. The results in this study support the work of Wang et al. (2016), but the application of the algorithm to more radars in the SuperDARN network with different positions and look directions is required to confirm the IMF By dependence.

5.4. Seasonal Variation of Zonal Flow Channels

Figure 4 shows a bimodal distribution, with peaks close to the spring and autumn equinoxes. This distribution is likely influenced by the peaks in geomagnetic activity around the equinoxes due to the Russell-McPherron effect (Russell & McPherron, 1973). This effect describes the semiannual variation of geomagnetic activity due to the southward component of the IMF becoming statistically more geoeffective around the equinoxes. A similar distribution is also observed for the PIFs in Provan et al. (1999). Our results contain flow channels on both newly opened and old opened field lines, and this monthly distribution indicates a link between reconnection signatures in the majority of cases, regardless of whether the dayside features that can be seen are PIFs or another phenomena.

6. Conclusions

Our algorithm to detect flow channels within the polar cap (Herlingshaw et al., 2019) was applied to 2 years of data from the SuperDARN LYR radar. The algorithm identified 1,048 flow channels. The majority of the FCs were located on the dayside, peaking between 9 and 12 MLT, but there were also events present around the dawn and dusk flanks and on the nightside. In this study, we focused on channels formed by dayside reconnection, close to the cusp/throat region, and deeper into the polar cap. The events were then filtered to $06 \leq MLT \leq 18$, which left 998 events remaining. The main findings of the study can be summarized as follows:

- The majority of the flow channels were short, variable pulses of 3 min in duration.
- The FCs were typically between 200 and 300 km in latitudinal width with peak velocities of 1.1–1.3 km s^{-1}.
- At lower peak velocities (<1.5 km s^{-1}), the spread in width is broad (72–660 km. Above this threshold, there are fewer fast, wide channels which suggests that higher velocity flows in the polar cap concentrate into localized, narrower channels.
- The flow channel location shows an IMF By dependence. The FC location is pushed dawnward for +By with mostly westward flows and duskward for −By with mostly eastward flows.
- The monthly FC occurrence shows a bimodal distribution with peaks around the equinoxes, likely due to increased solar wind-magnetospheric coupling at these times as described by the Russell-McPherron effect.

The coverage of the SuperDARN Longyearbyen radar was ideally situated for studying dayside zonal flows between 76 and 82° latitude (magnetic coordinates). In our future work, we will extend the algorithm to all SuperDARN radars within the polar cap in both hemispheres. This will allow us to understand the temporal evolution of flow channels across the entire polar cap region, the driving factors involved from the solar wind, and any interhemispheric asymmetries.

Data Availability Statement

Solar wind and IMF data are available at the Goddard Space Flight Center Space Physics Data Facility (https://cdaweb.sci.gsfc.nasa.gov/index.html/). The flow channel database generated for this paper is available online (https://figshare.com/articles/Flow_Channels_Detected_in_SuperDARN_Longyearbyen_data_2016-2018/12482642).

Acknowledgments
Financial support was provided by the Research Council of Norway under Contract 223252. The authors acknowledge the use of SuperDARN data, which are available online (http://vt.superdarn.org/). SuperDARN is a collection of radars funded by the national scientific funding agencies of Australia, Canada, China, France, Italy, Japan, Norway, South Africa, United Kingdom, and United States.

References

Andalsvik, Y., Sandholt, P., & Farrugia, C. (2011). Dayside and nightside contributions to cross-polar cap potential variations: The 20 March 2001 ICME case. *Annales Geophysicae*, *29*, 2189–2201. https://doi.org/10.5194/angeo-29-2189-2011

Carlson, H. C. (2012). Sharpening our thinking about polar cap ionospheric patch morphology, research, and mitigation techniques. *Radio Science*, *47*, 4RS0L21. https://doi.org/10.1029/2011RS004946

Carlson, H., Moen, J., Oksavik, K., Nielsen, C., Mccrea, I., Pedersen, T., & Gallop, P. (2006). Direct observations of injection events of subauroral plasma into the polar cap. *Geophysical Research Letters*, *33*, L05103. https://doi.org/10.1029/2005GL025230

Chisham, G., Lester, M., Milan, S. E., Freeman, M. P., Bristow, W. A., Grocott, A., & Walker, A. D. (2007). A decade of the Super Dual Auroral Radar Network (SuperDARN): Scientific achievements, new techniques and future directions. *Surveys in Geophysics*, *28*(1), 33–109. https://doi.org/10.1007/s10712-007-9017-8

Cousins, E. D. P., & Shepherd, S. G. (2010). A dynamical model of high-latitude convection derived from SuperDARN plasma drift measurements. *Journal of Geophysical Research*, *115*, A12329. https://doi.org/10.1029/2010JA016017

Cowley, S., & Lockwood, M. (1992). Excitation and decay of solar-wind driven flows in the magnetosphere-ionosphere system. *Annales Geophysicae*, *10*, 103–115.

Davies, J. A., Yeoman, T. K., Rae, I. J., Milan, S. E., Lester, M., Lockwood, M., & McWilliams, A. (2002). Ground-based observations of the auroral zone and polar cap ionospheric responses to dayside transient reconnection. *Annales Geophysicae*, *20*(6), 781–794. https://doi.org/10.5194/angeo-20-781-2002

Dungey, J. W. (1961). Interplanetary magnetic field and the auroral zones. *Physical Review Letters*, *6*, 47–48. https://doi.org/10.1103/PhysRevLett.6.47

Greenwald, R. A., Baker, K. B., Dudeney, J. R., Pinnock, M., Jones, T. B., Thomas, E. C., & Yamagishi, H. (1995). DARN/SuperDARN. *Space Science Reviews*, *71*(1–4), 761–796. https://doi.org/10.1007/BF00751350

Haerendel, G., Paschmann, G., Sckopke, N., Rosenbauer, H., & Hedgecock, P. C. (1978). The frontside boundary layer of the magnetosphere and the problem of reconnection. *Journal of Geophysical Research*, *83*(A7), 3195–3216. https://doi.org/10.1029/JA083iA07p03195

Heelis, R. A. (1984). The effects of interplanetary magnetic field orientation on dayside high-latitude ionospheric convection. *Journal of Geophysical Research*, *89*(A5), 2873–2880. https://doi.org/10.1029/JA089iA05p02873

Heppner, J. P., & Maynard, N. C. (1987). Empirical high-latitude electric field models. *Journal of Geophysical Research*, *92*(A5), 4467–4489. https://doi.org/10.1029/JA092iA05p04467

Herlingshaw, K., Baddeley, L., Oksavik, K., Lorentzen, D., & Bland, E. (2019). A study of automatically detected flow channels in the polar cap ionosphere. *Journal of Geophysical Research: Space Physics*, *124*, 9430–9447. https://doi.org/10.1029/2019JA026916

Hosokawa, K., Zou, Y., & Nishimura, Y. (2019). Airglow patches in the polar cap region: A review. *Space Science Reviews*, *215*, 53. https://doi.org/10.1007/s11214-019-0616-8

Karlson, K. A., Øieroset, M., Moen, J., & Sandholt, P. E. (1996). A statistical study of flux transfer event signatures in the dayside aurora: The IMF B_y-related prenoon-postnoon symmetry. *Journal of Geophysical Research*, *101*(A1), 59–68. https://doi.org/10.1029/95JA02590

Koustov, A. V., Ullrich, S., Ponomarenko, P. V., Nishitani, N., Marcucci, F. M., & Bristow, W. A. (2019). Occurrence of F region echoes for the polar cap SuperDARN radars. *Earth, Planets and Space*, *71*(1), 112.

Lockwood, M., Cowley, S. W. H., Sandholt, P. E., & Lepping, R. P. (1990). The ionospheric signatures of flux transfer events and solar wind dynamic pressure changes. *Journal of Geophysical Research*, *95*(A10), 17,113–17,135. https://doi.org/10.1029/JA095iA10p17113

Lockwood, M., Milan, S. E., Onsager, T., Perry, C. H., Scudder, J. A., Russell, C. T., et al. (2001). Cusp ion steps, field-aligned currents and poleward moving auroral forms. *Journal of Geophysical Research*, *106*(A12), 29,555–29,569. https://doi.org/10.1029/2000JA900175

MacDougall, J. W., & Jayachandran, P. T. (2001). Polar cap convection relationships with solar wind. *Radio Science*, *36*(6), 1869–1880. https://doi.org/10.1029/2001RS001007

Moen, J., Oksavik, K., Alfonsi, L., Rinne, Y., Romano, V., & Spogli, L. (2013). Space weather challenges of the polar cap ionosphere. *Journal of Space Weather and Space Climate*, *3*, A02. https://doi.org/10.1051/swsc/2013025

Neudegg, D., Cowley, S., Milan, S., Yeoman, T., Lester, M., Provan, G., & Georgescu, E. (2000). A survey of magnetopause FTEs and associated flow bursts in the polar ionosphere. *Annales Geophysicae*, *18*, 416–435. https://doi.org/10.1007/s005850050900

Nishimura, Y., Lyons, L. R., Zou, Y., Oksavik, K., Moen, J. I., Clausen, L. B., & Lester, M. (2014). Day-night coupling by a localized flow channel visualized by polar cap patch propagation. *Geophysical Research Letters*, *41*, 3701–3709. https://doi.org/10.1002/2014GL060301

Nishimura, Y., Lyons, L. R., Zou, S., Xing, X., Angelopoulos, V., Mende, S. B., & Heinselman, C. (2010). Preonset time sequence of auroral substorms: Coordinated observations by all-sky imagers, satellites, and radars. *Journal of Geophysical Research*, *115*, A00I08. https://doi.org/10.1029/2010JA015832

Oksavik, K., Barth, V. L., Moen, J., & Lester, M. (2010). On the entry and transit of high-density plasma across the polar cap. *Journal of Geophysical Research*, *115*, A12308. https://doi.org/10.1029/2010JA015817

Oksavik, K., Moen, J., & Carlson, H. C. (2004). High-resolution observations of the small-scale flow pattern associated with a poleward moving auroral form in the cusp. *Geophysical Research Letters*, *31*, L11807. https://doi.org/10.1029/2004GL019838

Pettigrew, E. D., Shepherd, S. G., & Ruohoniemi, J. M. (2010). Climatological patterns of high-latitude convection in the Northern and Southern Hemispheres: Dipole tilt dependencies and interhemispheric comparisons. *Journal of Geophysical Research*, *115*, A07305. https://doi.org/10.1029/2009JA014956

Pinnock, M., Rodger, A. S., Dudeney, J. R., Baker, K. B., Newell, P. T., Greenwald, R. A., & Greenspan, M. E. (1993). Observations of an enhanced convection channel in the cusp ionosphere. *Journal of Geophysical Research*, *98*(A3), 3767–3776. https://doi.org/10.1029/92JA01382

Provan, G., Yeoman, T. K., & Cowley, S. W. H. (1999). The influence of the IMF B_y component on the location of pulsed flows in the dayside ionosphere observed by an HF radar. *Geophysical Research Letters*, *26*(4), 521–524. https://doi.org/10.1029/1999GL900009

Provan, G., Yeoman, T., & Milan, S. (1998). CUTLASS Finland radar observations of the ionospheric signatures of flux transfer events and the resulting plasma flows. *Annales Geophysicae*, *16*, 1411–1422. https://doi.org/10.1007/s00585-998-1411-0

Rinne, Y., Moen, J., Baker, J. B. H., & Carlson, H. C. (2011). Convection surrounding mesoscale ionospheric flow channels. *Journal of Geophysical Research*, *116*, A05213. https://doi.org/10.1029/2010JA015997

Rinne, Y., Moen, J., Carlson, H. C., & Hairston, M. R. (2010). Stratification of east-west plasma flow channels observed in the ionospheric cusp in response to IMF B_Y polarity changes. *Geophysical Research Letters*, *37*, L13102. https://doi.org/10.1029/2010GL043307

Ruohoniemi, J. M., & Greenwald, R. A. (1996). Statistical patterns of high-latitude convection obtained from Goose Bay HF radar observations. *Journal of Geophysical Research*, *101*(A10), 21,743–21,763. https://doi.org/10.1029/96JA01584

Ruohoniemi, J. M., & Greenwald, R. A. (2005). Dependencies of high-latitude plasma convection: Consideration of interplanetary magnetic field, seasonal, and universal time factors in statistical patterns. *Journal of Geophysical Research*, *110*, A09204. https://doi.org/10.1029/2004JA010815

Russell, C. T., & Elphic, R. C. (1978). Initial ISEE magnetometer results: Magnetopause observations (Article published in the special issues: Advances in Magnetospheric Physics with GEOS- 1 and ISEE - 1 and 2.) *Space Science Reviews*, *22*(6), 681–715. https://doi.org/10.1007/BF00212619

Russell, C. T., & Elphic, R. C. (1979). ISEE observations of flux transfer events at the dayside magnetopause. *Geophysical Research Letters*, *6*(1), 33–36. https://doi.org/10.1029/GL006i001p00033

Russell, C. T., & McPherron, R. L. (1973). Semiannual variation of geomagnetic activity. *Journal of Geophysical Research*, *78*(1), 92–108. https://doi.org/10.1029/JA078i001p00092

Sandholt, P., Andalsvik, Y., & Farrugia, C. (2010). Polar cap flow channel events: Spontaneous and driven responses. *Annales Geophysicae*, *28*, 2015–2025. https://doi.org/10.5194/angeo-28-2015-2010

Sandholt, P., & Farrugia, C. (2009). Plasma flow channels at the dawn/dusk polar cap boundaries: Momentum transfer on old open field lines and the roles of IMF By and conductivity gradients. *Annales Geophysicae*, *27*, 1527–1554. https://doi.org/10.5194/angeo-27-1527-2009

Sandholt, P., Farrugia, C., & Andalsvik, Y. (2010). Polar cap convection/precipitation states during Earth passage of two ICMEs at solar minimum. *AGU Fall Meeting Abstracts*, *28*(4), 1023–1042.

Spicher, A., Clausen, L. B. N., Miloch, W. J., Lofstad, V., Jin, Y., & Moen, J. I. (2017). Interhemispheric study of polar cap patch occurrence based on Swarm in situ data. *Journal of Geophysical Research: Space Physics*, *122*, 3837–3851. https://doi.org/10.1002/2016JA023750

Thomas, E. G., & Shepherd, S. G. (2018). Statistical patterns of ionospheric convection derived from mid-latitude, high-latitude, and polar SuperDARN HF radar observations. *Journal of Geophysical Research: Space Physics*, *123*, 3196–3216. https://doi.org/10.1002/2018JA025280

Wang, B., Nishimura, Y., Lyons, L., Zou, Y., Carlson, H., Frey, H., & Mende, S. (2016). Analysis of close conjunctions between dayside polar cap airglow patches and flow channels by all-sky imager and DMSP. *Earth, Planets and Space*, *68*, 150. https://doi.org/10.1186/s40623-016-0524-z

Yeoman, T., Hanlon, P., & McWilliams, K. (2002). Letter to the editor A statistical study of the location and motion of the HF radar cusp. *Annales Geophysicae*, *20*, 275–280. https://doi.org/10.5194/angeo-20-275-2002

Zou, Y., Nishimura, Y., Lyons, L. R., Shiokawa, K., Donovan, E. F., Ruohoniemi, J. M., & Nishitani, N. (2015). Localized polar cap flow enhancement tracing using airglow patches: Statistical properties, IMF dependence, and contribution to polar cap convection. *Journal of Geophysical Research: Space Physics*, *120*, 4064–4078. https://doi.org/10.1002/2014JA020946